Mar Geophys Res
DOI 10.1007/s11001-010-9102-0

Evolution of errors in the altimetric bathymetry model used by Google Earth and GEBCO

K. M. Marks • W. H. F. Smith • D. T. Sandwell

Received: 14 May 2010/ Accepted: 5 October 2010

Abstract We analyze errors in the global bathymetry models of Smith and Sandwell that combine satellite altimetry with acoustic soundings and shorelines to estimate depths. Versions of these models have been incorporated into Google Earth and the General Bathymetric Chart of the Oceans (GEBCO). We use Japan Agency for Marine-Earth Science and Technology (JAMSTEC) multibeam surveys not previously incorporated into the models as "ground truth" to compare against model versions 7.2 through 12.1, defining vertical differences as "errors." Overall error statistics improve over time: 50th percentile errors declined from 57 to 55 to 49 m, and 90th percentile errors declined from 257 to 235 to 219 m, in versions 8.2, 11.1 and 12.1. This improvement is partly due to an increasing number of soundings incorporated into successive models, and partly to improvements in the satellite gravity model. Inspection of specific sites reveals that changes in the algorithms used to interpolate across survey gaps with altimetry have affected some errors. Versions 9.1 through 11.1 show a bias in the scaling from gravity in milliGals to topography in meters that affected the 15-160 km wavelength band. Regionally averaged (>160 km wavelength) depths have accumulated error over successive versions 9 through 11. These problems have been mitigated in version 12.1, which shows no systematic variation of errors with depth. Even so, version 12.1 is in some respects not as good as version 8.2, which employed a different algorithm.

Keywords Errors • Satellite bathymetry • Bathymetric grids • Google Earth • GEBCO • Multibeam

K. M. Marks • W. H. F. Smith
NOAA Laboratory for Satellite Altimetry
Silver Spring, MD 20910, USA
e-mail: Karen.Marks@noaa.gov

D. T. Sandwell
Scripps Institution of Oceanography, La Jolla, CA 92093, USA

Published online: 09 November 2010

Introduction

A variety of applications in biology, education, geology, and oceanography need a model of worldwide ocean depths. The raw material for such a model-bathymetric survey data- are increasingly made public, and many recent surveys have been stimulated by the potential for new territorial claims under the Law of the Sea. New swath mapping and imaging techniques generate great quantities of bathymetric data. Even so, the global ocean remains poorly covered by soundings, and the majority of acoustic data in the remote basins are older, more error-prone, and poorly navigated data (Smith 1993). Comparisons of sounding controls used in both older and newer versions of Smith and Sandwell's (1997) bathymetric model show that despite extensive contributions of new data from numerous government and research organizations, 35% of the ocean area still lies more than 10 km from a sounding, which is only a small improvement over 40% a decade ago. The problem is that most of the new surveys are covering areas that were previously mapped, albeit with older technology, because there is no program dedicated to systematic mapping of the oceans. Only 15% of the area in the current 1-min Mercator grid bathymetry model is constrained by soundings; the other 85% of the ocean remains indirectly mapped by some interpolation scheme. Gaps as large as 10^5 km^2 must be filled.

Satellite altimeters cover the oceans with uniformly distributed resolution and at a far greater density (track

Table 1 Bathymetry grid attributes

Version	Released	Spacing	Node	Projection	Coverage	Gravity	Notes
S&S 7.2	June 1997	2' longitude	pixel	Mercator	± 72°	7.2	Smith and Sandwell (1997)
S&S 8.2	Nov. 2000	2' longitude	pixel	Mercator	± 72°	9.2	Refined transfer function
S2004[a]	Apr. 2004	1'	grid	geographic	global	9.2*	8.2 below 1000 m and equatorward of 72°, GEBCO[b] in shallow water and polar regions
S&S 9.2	Apr. 2007	2' longitude	pixel	Mercator	± 80.738°	16.1	New data added, NOAA, NGA, NAVO, SIO effort
S&S 9.1	Aug. 2007	1' longitude	pixel	Mercator	± 80.738°	16.1	Changed to 1' grid
S&S 10.1	May 2008	1' longitude	pixel	Mercator	± 80.738°	16.1	Bad track editing
SRTM30_Plus V4.0	May 2008	30 arc-seconds	pixel	geographic	global	16.1*	Based on S&S 10.1, limited data editing, used in Google Earth
S&S 11.1	Sept. 2008	1' longitude	pixel	Mercator	± 80.738°	16.1	Editing and new data added
SRTM30_Plus V5.0	Sept. 2008	30 arc-seconds	pixel	geographic	global	16.1*	Based on S&S 11.1, includes IBCAO[c] V2.0 north of 80°N
GEBCO_08[d] V20081212	Dec. 2008	30 arc-seconds	pixel	geographic	global	16.1*	SRTM30_Plus V5.0 and other data
GEBCO_08[d] V20090130	Jan. 2009	30 arc-seconds	pixel	geographic	global	16.1*	Artifacts removed
GEBCO_08[d] V20090202	Feb. 2009	30 arc-seconds	pixel	geographic	global	16.1*	Artifacts removed
GEBCO_08[d] V20091120	Nov. 2009	30 arc-seconds	pixel	geographic	global	16.1*	SRTM30_Plus V5.0, combined with IBCAO[c] V2.23 north of 64°N and other data
S&S 12.1	Aug. 2009	1' longitude	pixel	Mercator	± 80.738°	18.1	Scaling correction and initialization from S2004[a]
SRTM30_Plus V6.0	Nov. 2009	30 arc-seconds	pixel	geographic	global	18.1*	Based on S&S 12.1, includes IBCAO[c] V2.23 north of 80°N

* Only Smith and Sandwell (S&S) bathymetry models derive depths from satellite gravity data and combine them with acoustic soundings and shorelines. Geographic bathymetry grids are resampled from S&S Mercator projection models.
[a] Smith (unpublished); ftp://falcon.grdl.noaa.gov/pub/walter/Gebco_SandS_blend.bi2
[b] British Oceanographic Data Center (2003)
[c] Jakobsson et al. (2008)
[d] http://www.gebco.net

spacing about 4 km) than ship surveys. The altimeters measure sea surface height, from which gravity anomalies may be derived and seafloor structure inferred. Therefore there have been many efforts to estimate regional and global bathymetric models by exploiting altimetry to interpolate between soundings (Baudry and Calmant 1991; Calmant 1994; Jung and Vogt 1992; Ramillien and Cazenave 1997; Sichoix and Bonneville 1996; Smith and Sandwell 1994, 1997).

The Smith and Sandwell (1997) bathymetric model and its updates have been widely used in the scientific community for more than a decade, and recently it has been incorporated into the GEBCO_08 and SRTM30_Plus products (Becker et al. 2009), and the popular web application Google Earth. Over the years, there have been numerous updates to the model (see Table 1) as more ship data became available and as modeling techniques evolved. However, until this study, there has been no published comparison of each updated version to its predecessor, or to multibeam data that became available after a version was released. It is important to perform systematic evaluations of the model updates in order to identify errors and assess accuracy, and to confirm the model is being improved.

In this paper, we compare Smith and Sandwell bathymetric model versions 7.2 through 12.1 against Japan Agency for Marine-Earth and Science Technology (JAMSTEC) multibeam acoustic swath

survey data that were not available when the models were prepared (or were withheld in this study for testing purposes). The JAMSTEC data are concentrated in the western Pacific Ocean, but they are also located in the eastern Indian Ocean, the Arctic Ocean north of Alaska, parts of the southern and eastern Pacific Ocean, there is a cruise in the Southeast Indian Ocean, and there are also cruises that nearly circumnavigate the globe along about 15° or 30° S latitudes. These data cover a number of geologic settings and we chose sites that covered both smooth and rough areas and traversed gaps in the control data used in the models. We consider the differences between the model depths and JAMSTEC "ground truth" data to be "errors," and for purposes of this study "overall" is the aggregate of these data. We find that overall errors are being reduced in successive bathymetry model updates. However, our examination of local areas having large gaps between tracks has revealed problems with the bathymetry prediction algorithm that are otherwise inconspicuous when errors are analyzed on a global scale. Correcting these algorithm problems leads to improved bathymetric models and to better global statistics as well.

History of the bathymetric model

The Smith and Sandwell (1997) bathymetric model combines depths derived from satellite gravity data with in-situ data such as soundings and shorelines. This approach is advantageous because satellite tracks cover the ocean more densely than ship tracks, which have only sparse coverage. In the bathymetric model, gaps between ship measurements are filled in with derived depths by a method described in detail in Smith and Sandwell (1994). An overview of the method is that gravity anomalies are Gaussian filtered to pass full wavelengths <160 km, and then converted to bathymetry with a gravity-to-topography scaling factor assuming appropriate geologic properties locally calibrated by ship soundings. The predicted bathymetry is then combined with regional low-pass filtered (passing full wavelengths >160 km) bathymetric soundings to form the altimetric bathymetry model. The gravity-to-topography scaling factor is estimated from the empirical ratio of band-pass filtered soundings to band-pass filtered, downward-continued gravity anomalies, in the prediction (15-160 km) band. Gravity and bathymetry may be correlated in the prediction band, if sediment is thin and seafloor relief is high enough; at longer wavelengths the seafloor topography is usually isostatically compensated and shows little or no correlation with gravity. In most areas, the scaling factor implies a geologically reasonable density contrast at the seafloor. Exceptions occur over very tall seamounts, where a linear filtering process cannot be adequate to characterize the relationship between depth and gravity (Parker 1973).

When the bathymetric model is periodically updated, a new version is released. The successive versions of the model examined in this study are listed in Table 1. The updated versions use the latest satellite gravity field available to improve bathymetry from the prediction band, and the incorporation of additional soundings produces a better local gravity-to-topography scale factor. There were also changes in the modeling technique. At the time of Smith and Sandwell's 1994 paper, dense satellite altimeter data from the Geosat Geodetic Mission were only available south of 30°S, and the majority of the sparse echo soundings in the southern oceans were poorly navigated (Smith 1993). In July 1995 the U.S. Navy released all the Geosat Geodetic Mission data. These were combined with ERS-1 data and processed into a gravity anomaly field covering ±72° latitude (Sandwell and Smith 1997) and a depth model (version 7.2; Smith and Sandwell 1997). The depth model employed the same technique as in Smith and Sandwell (1994), but adapted to a Mercator grid covering the wider latitude range. Since many of the soundings available in the more northern oceans were well navigated, an additional step was added to the algorithm. In this step, after obtaining the results as in the 1994 method, the result may be perturbed to fit designated trusted soundings. Grid cells were therefore marked as either constrained by soundings or interpolated by altimetry in that and subsequent products.

Comments on version 7.2 included criticism of an "orange peel" texture, a random bumpiness, in the abyssal areas of the model. While later work (Goff and Smith 2003; Goff et al. 2004) showed that this bumpy texture contained information about real abyssal hill fabric, version 8.2 took steps to suppress it. An inversion scheme, following Oldenburg (1974), was used to convert band-pass filtered and downward-continued gravity into depth. This scheme accounted for the higher-order non-linearities of Parker (1973) and also included a threshold: gravity anomalies were not fit unless they exceeded a threshold value, set to the root-mean-square amplitude of the filtered gravity over abyssal areas. In this way the orange peel texture was suppressed. We find in this paper that the algorithm also may have done a particularly good job of estimating seamount heights, due to its accounting for the non-linear terms at tall features.

After topography version 8.2 in November 2000, effort shifted toward the reprocessing of radar altimeter data to improve the signal to noise ratio in the derived gravity data (Sandwell and Smith 2005, 2009). These allowed the gravity to be produced on a 1 arc-minute

Mercator grid and expanded from ±72° to ±81° latitude, and eventually implied that the high-cut filter used in bathymetry prediction could be allowed to pass shorter wavelengths. In 2005, the *USS San Francisco* nuclear attack submarine collided with a seamount south of Guam. Although this seamount was not shown on the navigation products used by the U.S. Navy at that time, a seamount in that area was expressed in the version 8.2 bathymetry model. This collision stimulated new efforts to improve both the gravity and bathymetry models. In order to produce new models quickly, the old 1994 and 1997 algorithms were employed, rather than the non-linear, iterative, and threshold-employing scheme that had been used for version 8.2.

The General Bathymetric Charts of the Oceans (GEBCO) grid has historically been based on bathymetric contours of the world's oceans that were originally available as a series of paper maps, and later as digital contours in the GEBCO digital atlas (British Oceanographic Data Center 2003). The S2004 bathymetry model combined Smith and Sandwell's (1997) version 8.2 with GEBCO as noted in Table 1. The SRTM30_Plus V4.0 model that was released in May 2008 and is used in Google Earth is essentially version 10.1 on a 30 arc-second geographic grid (SRTM30_Plus V5.0 is documented in Becker et al. 2009), although resampling the Mercator-projected Smith and Sandwell model onto a 30 arc-second grid does not produce a grid with higher resolution (Marks and Smith 2006). In 2008, GEBCO adopted SRTM30_Plus V5.0 for use in its digital gridded terrain and ocean model.

Multibeam data

We obtained multibeam echo sounder data as *xyz* ping files from the JAMSTEC web site (cited in Acknowledgements). Swaths we examine are KR05-01 from R/V *Kairei* and MR06-01 from R/V *Mirai* collected in 2005 and 2006, respectively. Both vessels used a Sena Advanced Integrated Navigation System (data format version 02.6) and a Seabeam 2112.004 multibeam system, the latter of which has a manufacturer-listed accuracy of up to 0.5% of depth. The multibeam data were processed, cleaned, and quality controlled using HIPS/SIPS 5.3 (CARIS) software. Processing included rejecting side beams (beam numbers 1-12 and 131-151), rejecting spike noise data, deleting location error data, and converting to an ASCII format. Gravity measurements were from a Fuguro Bodenseewerk KSS 31 on R/V *Kairei*. The total magnitude gravity data were corrected for drift, the Eotvos effect, tagged with longitudes and latitudes where the measurements were made, and provided as ASCII files. We reduced the data to free-air gravity anomalies relative to the GRS80 Geodetic Reference System.

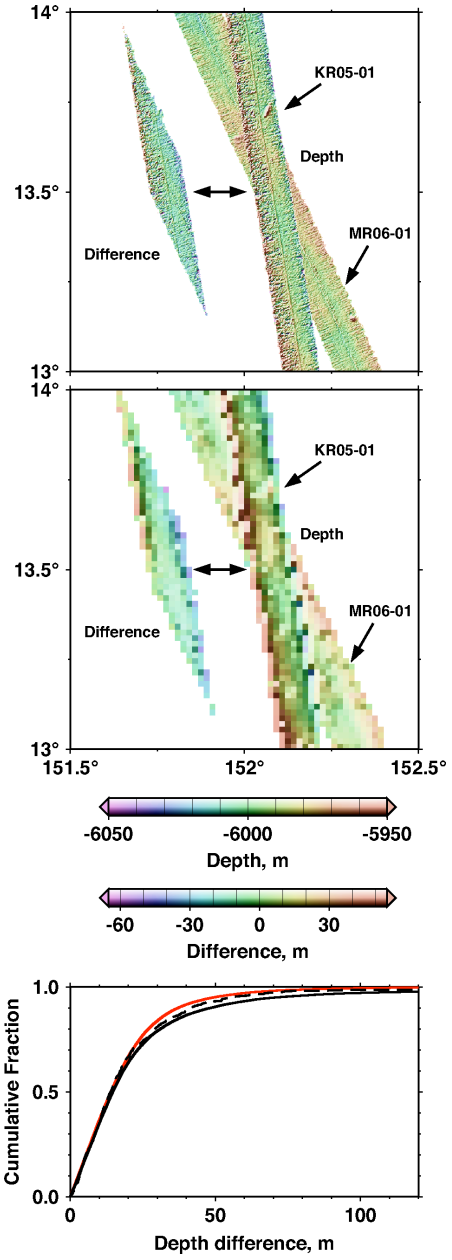

Fig. 1 Overlapping multibeam swaths KR05-01 and MR06-01 and their differences in depth where they intersect (the parallelogram-shaped areas) are plotted on a 6 arc-second grid (*top panel*), and the same but plotted as median depths on a 1-min Mercator grid (*middle panel*). A cumulative histogram (*bottom panel*) plots depth differences between KR05-01 and MR06-01 (*red line*), and between KR05-01 and combined MR06-01, MR99-K06, and MR00-K02 overlaps. The *solid black line* is from differences using a 6 arc-second grid, and the *dashed line* is the same from a 1 min grid

We plot swath multibeam data from KR05-01 and MR06-01 in Fig. 1 (top panel); they overlap in a study area we focus on later. We exploit this overlap to

assess the repeatability of these multibeam data using the method described in Marks and Smith (2009) whereby *xyz* depth points from swath MR06-01 are subtracted from a 6-arc second grid of the multibeam depths from KR05-01. These depth differences are plotted with a solid red line in a cumulative histogram (bottom panel). For these two overlapping multibeam swaths the standard deviation is 23.4 m and 95% of the depth differences are less than 49 m, or about 0.8% of depth. It happens that two other swaths (MR99-K06 and MR00-K02) also intersect KR05-01 nearby, and including the MR06-01 data we plot their *xyz* point depth differences with the KR05-01 grid with a solid black line in the cumulative histogram. We find that 95% of the depth differences are less than 67 m, or about 1.1% of depth. Apparently the depth differences are larger where MR99-K06 and MR00-K02 intersect KR05-01, possibly due to a roll bias in MR99-K06 (Marks and Smith 2009), or stretches of data collection that were not optimum. We note that depth differences between two other intersecting swaths (MR02-K01 and MR00-K008) in Marks and Smith (2009) had a standard deviation of 10.9 m and 95% of the differences were less than 19.3 m, which is about 0.47% of depth. It is possible that the scatter along the western edge of KR05-01 (see top panel) which is also evident in the enlarged image of the depth differences (top panel) is manifest in larger depth difference values. Perhaps more of the outer beams in KR05-01 should have been rejected in processing. We also gridded the swaths by taking their median depths on a 1-min mesh and plotted these, along with their median depth differences, in the middle panel of Fig. 1. The scatter is reduced by using median depths and accordingly 95% of the depth differences are less than 52 m (dashed black line on the cumulative histogram, lower panel).

Although we consider JAMSTEC multibeam data to be the standard against which depths from bathymetry models may be compared, even multibeam measurements suffer from errors and these may vary from place to place. Nevertheless, we use JAMSTEC multibeam data in both our global and local comparisons because of their good coverage, the fact that the data have been processed, cleaned and quality controlled, and because they are freely available for download in the form of ASCII *xyz* data files. Further, as we evaluate the successive bathymetry model versions the JAMSTEC data we compare them against remain the same, thus permitting us to also evaluate changes in the bathymetry model as it has evolved.

We note here that for bathymetry model versions 11.1 and 12.1 that had available JAMSTEC data incorporated, we created companion versions in which all JAMSTEC data were withheld. This enabled us to test errors in versions 11.1 and 12.1 as we describe in the following sections.

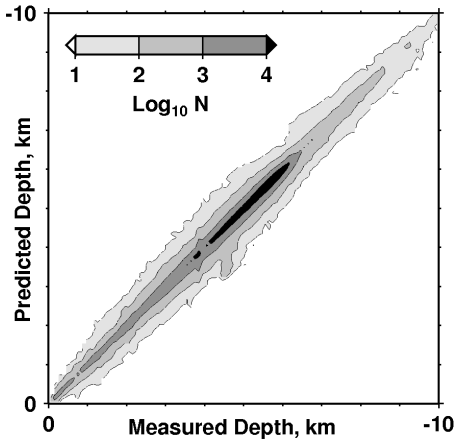

Fig. 2 Version 12.1 JAMSTEC controlled (measured) depths plotted against version 12.1 predicted depths (JAMSTEC withheld). The number of points (N) are contoured. Errors show no systematic variation with depth

Bathymetry model errors

Overall assessment

We make an overall assessment by looking at models built without JAMSTEC multibeam data, and comparing those models to the JAMSTEC soundings. The models are on 1-min Mercator grids, and the median of all available soundings in a grid cell is the value of the cell. Accordingly, we formed the median of all JAMSTEC multibeam data falling in 1-min Mercator grid cells, and subtracted these medians from the models' cell value.

We find that overall errors are being reduced in the successive bathymetry model updates. Errors are the differences between the updates and "ground truth" JAMSTEC multibeam surveys not previously incorporated into the model (as described above). For versions 8.2, 11.1, and 12.1, the 50th percentile errors have declined from 57 to 55 to 49 m, and 90th percentile errors have declined from 257 to 235 to 219 m, respectively (note that the distribution is not Gaussian). Much of the overall error improvement can be attributed to an increasing number of available ship soundings that are incorporated into the models, many arising as coastal nations survey offshore for Law of the Sea claims. Other significant contributions to global error improvement are careful editing of the sounding data (Becker et al. 2009) and improvements in the satellite gravity model. The most recent update, version 12.1, shows no systematic variation of errors with depth (see Fig. 2).

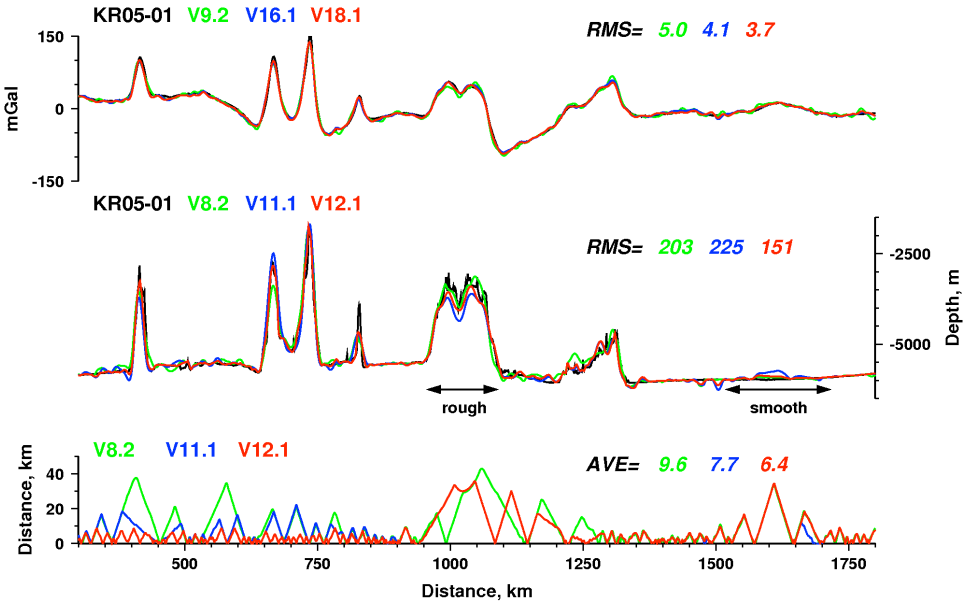

Fig. 3 Gravity (*top*), bathymetry (*middle*), and distance to nearest bathymetry control point (*bottom*) profiles along the track of ship survey KR05-01, comparing values measured by the ship with estimates from various altimetry models, indicated by *colored lines* and *labels*. RMS numbers are root-mean-square differences between altimetry model estimates and KR05-01 measurements. The areas labeled "smooth" and "rough" are examined in more detail in Figs. 6 and 9

Spectral Analyses

We chose a long (greater than 1,000 km) transit of the R/V *Kairei* during cruise KR05-01 for the analyses shown here. The profile we examine (Fig. 3) crosses a large part of the western Pacific, was continuously collected (no major course or speed changes, only one minor bend in the course of the ship), samples both rough seamounts and smooth abyssal plains, and in both smooth and rough areas the profile crosses areas where the nearest sounding control in the bathymetry models is more than 20 km away from the profile.

To plot and analyze the data as profiles we gridded the multibeam data onto a 6 arc-second grid and used GMT (Wessel and Smith 1998) routine "grdtrack" to sample the gridded multibeam bathymetry at the points where the gravity measurements were made. The latitude and longitude of these points were then projected into the Mercator coordinates used in the altimetric bathymetry models shown in Table 1 with the GMT routine "mapproject," and "grdtrack" was again used to sample these models at the KR05-01 gravity measurement points. Smith and Sandwell bathymetry model versions 8.2, 11.1, and 12.1 were so sampled, along with the corresponding gravity model versions 9.2, 16.1, and 18.1, from which they were built. We also computed the distance to the nearest control point in the bathymetry models and added that distance to the profile information as well.

Figure 3 shows the data we obtained along the profile. In the top panel, we have added 11 mGal to the gravity data reported by the ship in order to correct the mean level of the measurements; marine gravimeters are relative instruments and the absolute level usually needs correction (Wessel and Watts 1988). After adjustment of the mean level of the ship gravimeter values, we computed the root-mean-square (RMS) differences between the ship data and the three altimetric gravity models shown, obtaining 5.0, 4.1, and 3.7 for versions 9.2, 16.1, and 18.1, respectively. The middle panel shows the depth profiles and the RMS differences of 203, 225, and 151 for versions 8.2, 11.1, and 12.1, respectively. The bottom panel shows the distance to the nearest control in the bathymetry models. These distances are not the same in each version, as new data are added to newer versions and older data may be removed as editing evolves. Also, the increasing availability of multibeam data is reflected in the decreasing average distance from control (bottom panel) with newer bathymetry model version. However, we were able to identify areas of rough and smooth topography along the profile shown in Fig. 3 that were more than 20 km from the nearest control points in all the models. We present a closer look at these in the next section.

The portion of the profile data in Fig. 3 running from 350 to 1,400 km was selected for cross-spectral coherency analysis. This selection was made to encompass the large amplitude signals. The data sequences were resampled to a uniform 1-km sample spacing using GMT routine "sample1d" and then power spectral density (PSD) and cross-spectral coherency were computed using GMT routine "spectrum1d," which averages the periodograms obtained from successive overlapped and cosine-arch-tapered windows of the data series. We used a window length of 128 km, so that there are more than eight statistically independent samples contributing to our analysis.

The power spectral densities show that the gravity

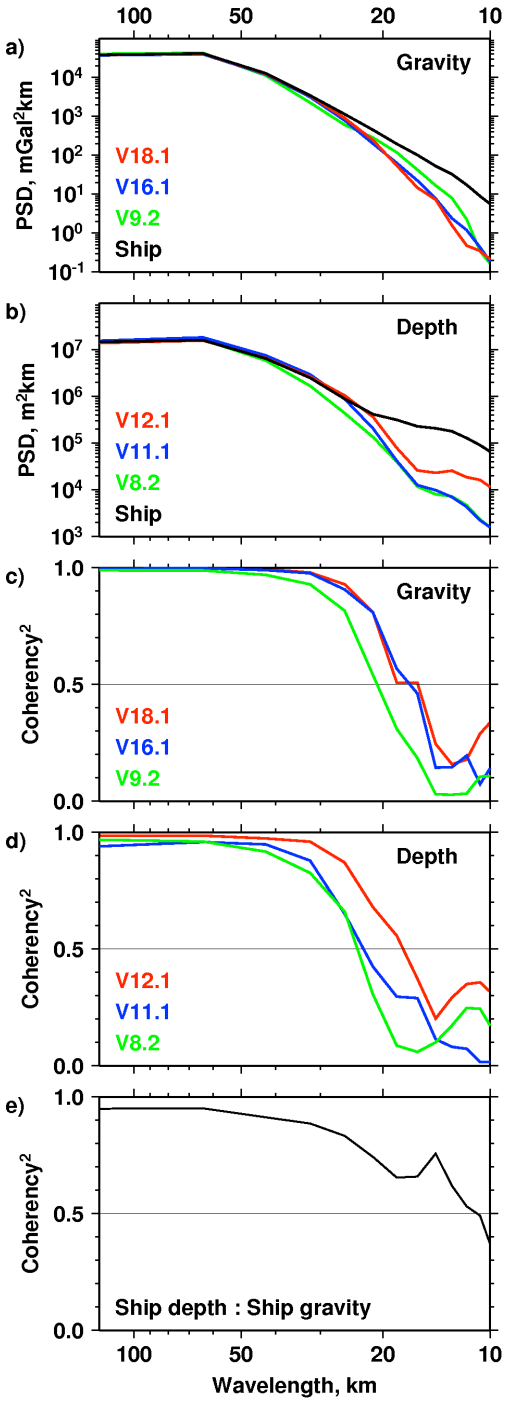

Fig. 4 Power spectral density (PSD) and cross-spectral coherency from the portion of the profiles shown in Fig. 3 that runs from 350 to 1,400 km. **a** Gravity PSD, **b** depth PSD, **c** gravity coherency, **d** depth coherency, and **e** coherency between gravity and depth as both are measured by KR05-01

(Fig. 4a) and bathymetry (Fig. 4b) measurements made on board the ship have more power than the corresponding model estimates at wavelengths shorter than 20 km. At wavelengths longer than 50 km, all the data show similar spectra. Between 20 and 50 km wavelengths, there are some differences.

The cross-spectral coherency between pairs of data sequences shown is the linear correlation coefficient as a function of wavelength, indicating how much of one sequence can be correlated with the other sequence through a linear filtering operation. Coherency near one indicates nearly perfect linear correlation of the two inputs, while coherency near zero indicates the absence of any significant linear process relationship between the two inputs. Interpretation of intermediate coherency values requires a priori knowledge or assumptions about the signal-to-noise ratio as a function of wavelength in either, or both, of the input sequences. If one input sequence is noise free while the other has noise, then the coherency is 0.5 where the signal-to-noise ratio in the noisy sequence is 1:1 (Bendat and Piersol 1986, Eq. 6.39). If both inputs have noise, uncorrelated with the signals and with each other, and both have the same signal-to-noise ratio as a function of wavelength, then the coherency is 0.25 when the signal-to-noise ratio is 1:1 (Bendat and Piersol 1986, Eq. 6.51).

The altimetric gravity models are strongly correlated with the ship's gravity measurements at wavelengths longer than 32 km (Fig. 4c), although coherency begins to decline at wavelengths shorter than 50 km. The coherency reaches 0.5 at a wavelength of 21 km for version 9.2 gravity, and at 18 km for versions 16.1 and 18.1. Since version 9.2 shows more power at these wavelengths than versions 16.1 or 18.1 (see Fig. 4a), this indicates that more of the power in version 9.2 was incoherent with the ship's gravity measurements. Thus, although versions 16.1 and 18.1 have less power than version 9.2, the power they do have is more coherent with the ship's measurements. The signal-to-noise ratio in the gravity models has improved between version 9 and version 16.

The altimetric bathymetry models are well correlated with the ship's depth measurements at wavelengths longer than 32 km (Fig. 4d), but coherency rolls off rapidly at shorter wavelengths. For both versions 8.2 and 11.1, coherency falls to 0.5 at 24 km wavelength, while for version 12.1 the corresponding wavelength is 18 km. Version 12.1 appears significantly better than version 11.1.

It is interesting to note that bathymetry version 8.2 does not show coherency significantly different than version 11.1 (Fig. 4d). In the next section we show that the RMS errors in version 8.2 are less than those in version 11.1 in both the smooth (Fig. 6) and rough (Fig. 9) areas where the distance to control is large; however, on the overall profile (Fig. 3) the RMS error of version 8.2 is higher than that of V11.1. The cross-spectral coherency analysis requires a long profile, and thus lumps together areas that are near to other control points with areas that are far from control points.

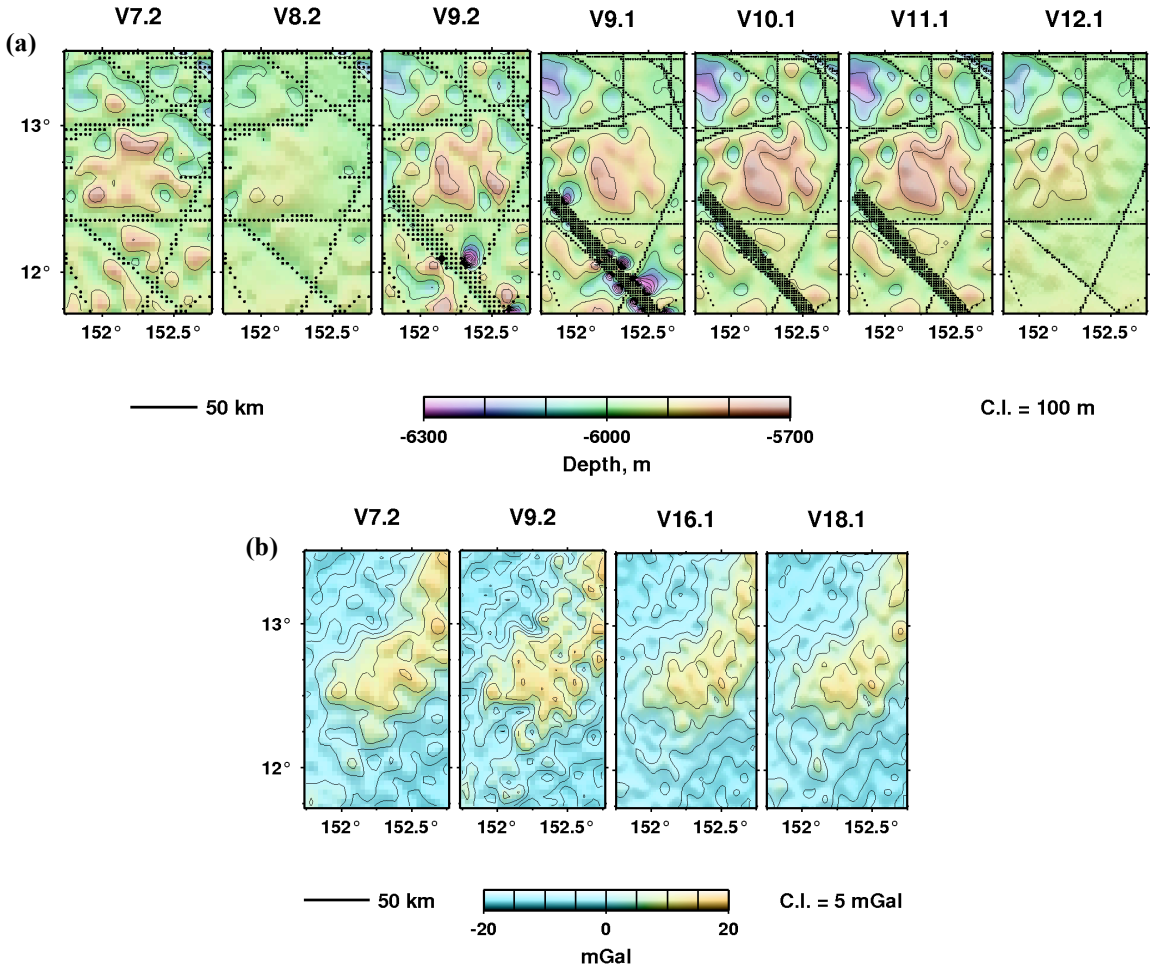

Fig. 5 **a** Bathymetric model versions and **b** satellite-derived gravity over smooth seafloor (Table 1 links gravity to bathymetry versions). *Black dots* are grid cells constrained by ship soundings. Short-wavelength gravity anomalies incorrectly give rise to corresponding bathymetry anomalies in versions 7.2, 9.2, 9.1, 10.1, and 11.1. Bathymetry version 8.2, which used a different algorithm, correctly suppressed the anomalies, and in 12.1 they are reduced by a scaling correction

In Fig. 4e, we computed the coherency between the ship's gravity and bathymetry measurements, which are both independent of altimetry. Because gravity can be sensitive to sub-seafloor structures, as well as structures perpendicular to the profile along the ship's path, we do not expect perfect correlation between these two series. Even so, the roll-off of coherency is much slower than in Fig. 4c and d, dropping to 0.5 at only 11 km wavelength. This implies that if the altimetric gravity field were sufficiently free of noise, or could capture more of the signal power at short wavelengths, then it could be used to obtain higher resolution (shorter wavelength) bathymetry estimates.

Errors over smooth seafloor

Here we focus on an area of smooth seafloor in the East Mariana Basin (Fig. 5) that has large gaps between surveys. Two multibeam swaths (KR05-01 and MR06-01) traverse this area (Fig. 6). Depths from these swaths were not incorporated into bathymetric model versions 11.1 and older because they were not yet available. These swaths span areas that have few depth soundings from other ships nearby.

Successive versions of the bathymetry model over smooth seafloor are shown in Fig. 5a, and satellite gravity anomalies are shown in Fig. 5b. In Fig. 6a we have plotted swaths KR05-01 and MR06-01 on the version 8.2 image, to demonstrate that the multibeam data show the seafloor is flat, and version 8.2 bathymetry is flat. Except in version 8.2, short-wavelength bathymetric anomalies in the center of the bathymetry versions shown in Fig. 5a increase in amplitude with successive model updates, even though the observed seafloor bathymetry is flat. These anomalies lie in a large area that is void of grid cells having ship constraints (black dots). The corresponding short-wavelength satellite gravity

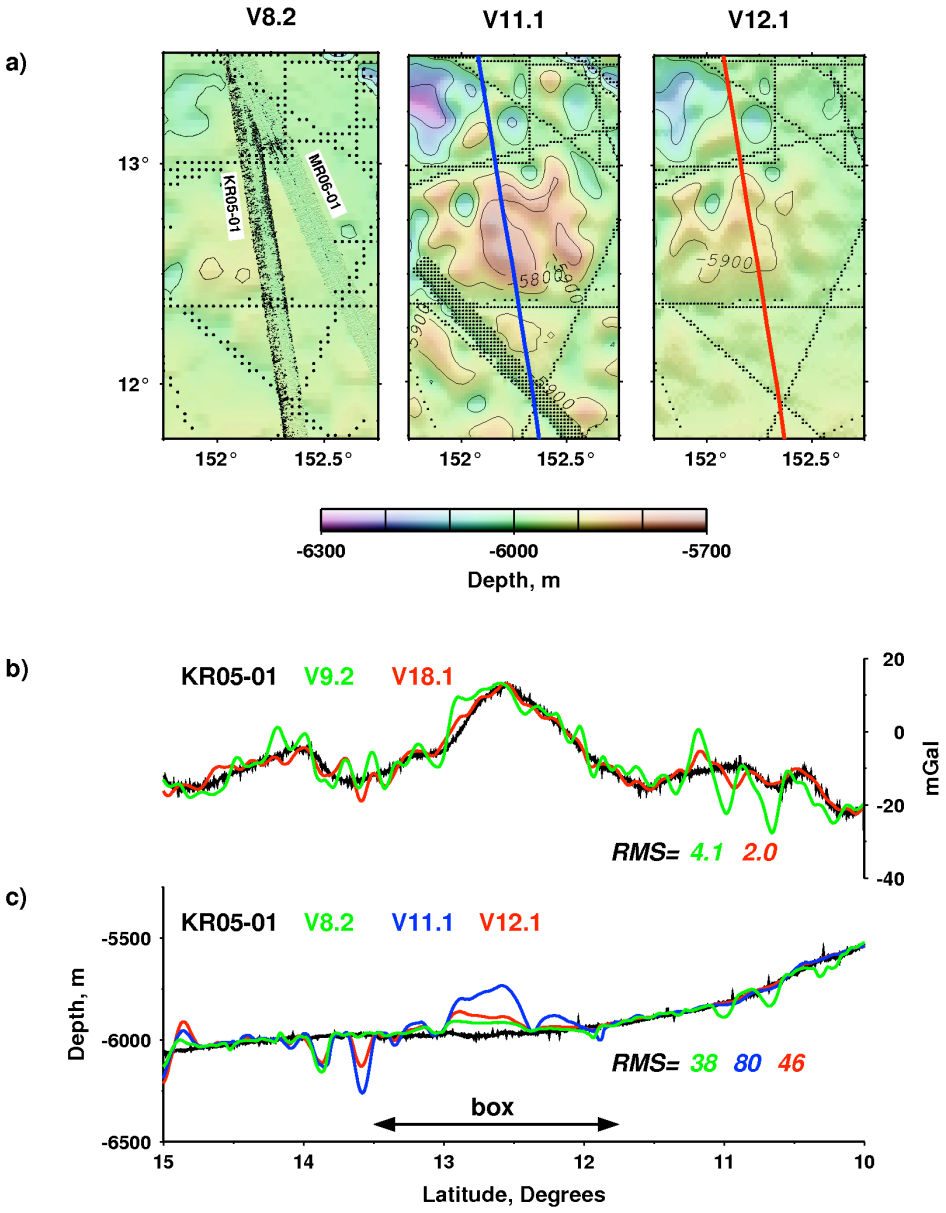

Fig. 6 **a** Selected bathymetry model versions over smooth seafloor. KR05-01 and MR06-01 multibeam data are plotted on version 8.2 image; multibeam shows seafloor is flat, and version 8.2 bathymetry is flat. Gravity (**b**) and bathymetry (**c**) profiles plotted along KR05-01 center-beam track. Satellite gravity version 18.1 is less noisy than 9.2 (RMS quantifies the differences between ship measurements and the models). Bathymetry version 8.2 matches measured depths best

anomalies (Fig. 5b), that most probably arise from sub-seafloor structure, are being incorrectly passed into the predicted bathymetry. Version 12.1 shown is one we created by withholding all JAMSTEC data, and which has improvements that led to its flatter bathymetry.

Gravity and bathymetry profiles are plotted along the KR05-01 center-beam track in Fig. 6b and c. The RMS differences between the ship data and corresponding altimetric models for the profile segment shown are notated on the figure. Even though newer version 18.1 satellite gravity anomalies are less noisy than those in version 9.2, depths predicted by bathymetry version 8.2 match KR05-01 depths better than more recent model updates (version 8.2 has the lowest RMS). This demonstrates how changes in the prediction algorithm used by the various bathymetry versions affects the accuracy of the resulting estimated depths, regardless of improved gravity input. We note that the RMS results shown in Fig. 3 are different (version 8.2 has an intermediate RMS value) than those shown in Fig. 6c (version 8.2 has the lowest RMS value). In Fig. 3 the RMS differences were calculated over the entirety of the profile shown, which spans a wide range of distances to control, while the profile in Fig. 6 is located where the distance to control is large (>20 km; the segment labeled “smooth” in Fig. 3 is enlarged in Fig. 6). So where controls are sparse and depths predicted from altimetry dominate (as is typical

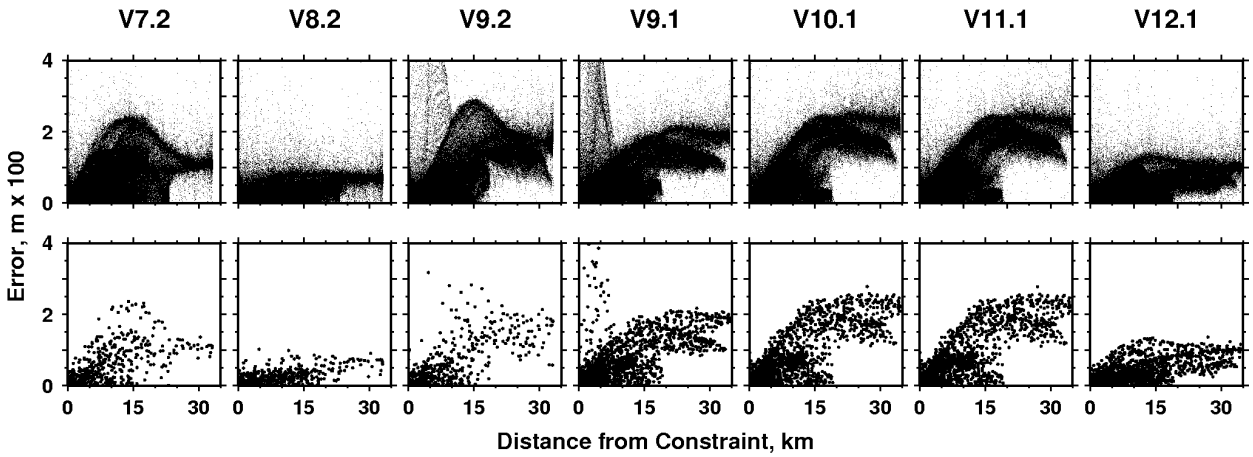

Fig. 7 Errors are the absolute value of the differences between KR05-01 and MR06-01 (located in Fig. 6a) multibeam depths and bathymetry models (Fig. 5a), plotted against distance to the nearest sounding constraining the prediction. The *top panel* plots errors for each multibeam point, the *bottom panel* plots errors from median multibeam depths calculated at the same spacing as the bathymetry grids. Scatter is reduced in the *bottom panel*. Large errors in versions 7.2, 9.2, 9.1, 10.1, and 11.1 result from a scaling problem. Corrected scaling in version 12.1 reduces errors. Version 8.2 used a different prediction algorithm that yields the lowest errors

over most of the oceans), the algorithm used in version 8.2 gave the best result.

To assess the errors in the bathymetric models over smooth seafloor, we calculated the differences between the *xyz* multibeam depth points from swaths KR05-01 and MR06-01 and the corresponding bathymetric model depths. This was done in two ways- one using every *xyz* point in the multibeam files provided by JAMSTEC, the other using median multibeam depths. In the second way the *xyz* data are projected into the Mercator coordinates used in the bathymetry model and the median is calculated using GMT routine "blockmedian" at the same grid spacing as the model. For each error the distance to the nearest sounding was calculated by searching the neighborhood for the nearest control point that is encoded in the bathymetry models. These errors for each *xyz* point are plotted against distance to the nearest sounding constraining the bathymetric model in Fig. 7 (top panel), and for each median multibeam depth (bottom panel). We see that the errors increase in amplitude with successive version- approaching 250 m in versions 10.1 and 11.1, while errors in versions 8.2 and 12.1 are only about 100 m. Further, the errors generally increase in amplitude with distance from constraint. These patterns persist even when the errors are from median multibeam depths, although taking medians reduces the overall amplitude. Most striking is how low the errors are in version 8.2, compared to the others. This is due to the threshold step in the special algorithm used in 8.2.

The amplified errors in versions 9, 10, and 11 can be explained by a scaling problem. The scaling problem arose inadvertently as a result of the transition from a 2-min grid spacing to a 1-min grid spacing. Recall that a gravity-to-topography scaling factor is used to convert satellite gravity anomalies to predicted bathymetry anomalies. When this scaling factor was estimated from soundings and satellite gravity based on 2-min grids, the shortest wavelengths in the bathymetry (~16 km, limited by the grid spacing) approximately matched the inherent ~15 km resolution of the gravity anomalies [shorter wavelengths are attenuated by upward continuation from the seafloor to the sea surface, and are also suppressed in the gravity calculation process (Sandwell and Smith 2009)]. However, when the grid spacing of the model was changed to 1-min, the shortest wavelengths in the bathymetry (~8 km) no longer matched the inherent ~15 km resolution of the gravity anomalies. This mismatch yielded an increased topographic variance that caused the gravity-to-topography scaling factor to be too large. The scaling problem is manifest as the incorrectly-amplified short-wavelength bathymetry anomalies seen in versions 9, 10, and 11 in Fig. 5a, and as the amplified errors seen the same versions in Fig. 7.

In version 12.1, the scaling problem was corrected by adjusting the short-wavelength cut-off of the filter applied to the 1-min gridded soundings to match the short-wavelength gravity resolution, for purposes of estimating the gravity-to-topography scaling factor. The result is flatter bathymetry anomalies as seen in version 12.1 in Fig. 5a, and smaller errors in the same version in Fig. 7.

Errors over rough seafloor

We performed the same assessment techniques as described above in a region of small seamounts in the East Mariana Basin that also has large gaps between

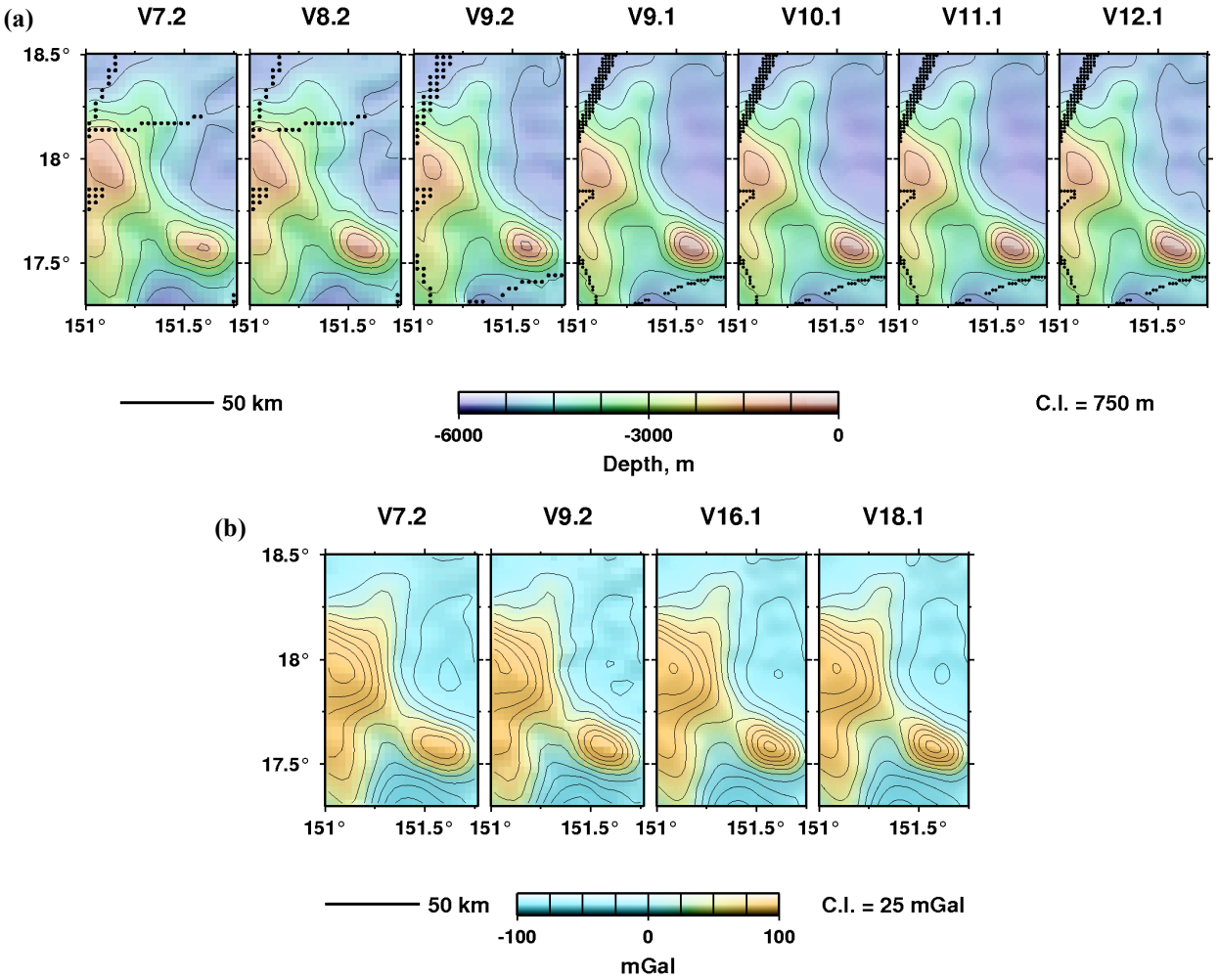

Fig. 8 **a** Bathymetric model versions and **b** satellite-derived gravity over rough seafloor. Table reference and *black dots* are the same as in Fig. 5 caption. Prediction-band (15-160 km) gravity anomalies are correctly passed into the bathymetry models

surveys; Fig. 8a plots the corresponding bathymetry model versions and Fig. 8b plots the satellite gravity anomalies. Multibeam depths from KR05-01 are plotted on the version 8.2 image in Fig. 9a. The swath path crosses the flank of one seamount and a ridge extending to an adjacent seamount, and there are only a few grid cells having ship control. The smooth bathymetry contours become jagged over the multibeam depths because very small-scale seafloor features can be resolved in the dense coverage multibeam affords. As before, version 12.1 shown is one with JAMSTEC multibeam tracks withheld.

In Fig. 8a all the bathymetry models appear similar, even though there are large distances between ship constraints. This is because the medium-wavelength satellite gravity anomalies lie within the 15-160 km prediction band and they are correctly passed by the gravity-to-topography transfer function into the bathymetry model versions. However a closer look at the bathymetry profiles along track KR05-01 (Fig. 9c) reveals that the seamount amplitude is predicted best by bathymetry version 8.2 that included the non-linearity between gravity and topography, which is important for capturing the amplitudes of seamounts (Marks and Smith 2007). The seamount amplitude is attenuated in versions 11.1 and 12.1 that did not include this feature in their prediction algorithms. Version 18.1 gravity anomalies (Fig. 9b) match the ship gravity best.

In Fig. 10 we see that the errors appear to increase with distance from constraint and also with successive model versions 9, 10, and 11, reaching ~ 800 m in versions 10 and 11. As we found in the smooth seafloor area, the errors are lowest (~500 m) in version 8.2 and close to that in the improved version 12.1. Errors from median multibeam depths (bottom panel) show less scatter and reduced amplitudes.

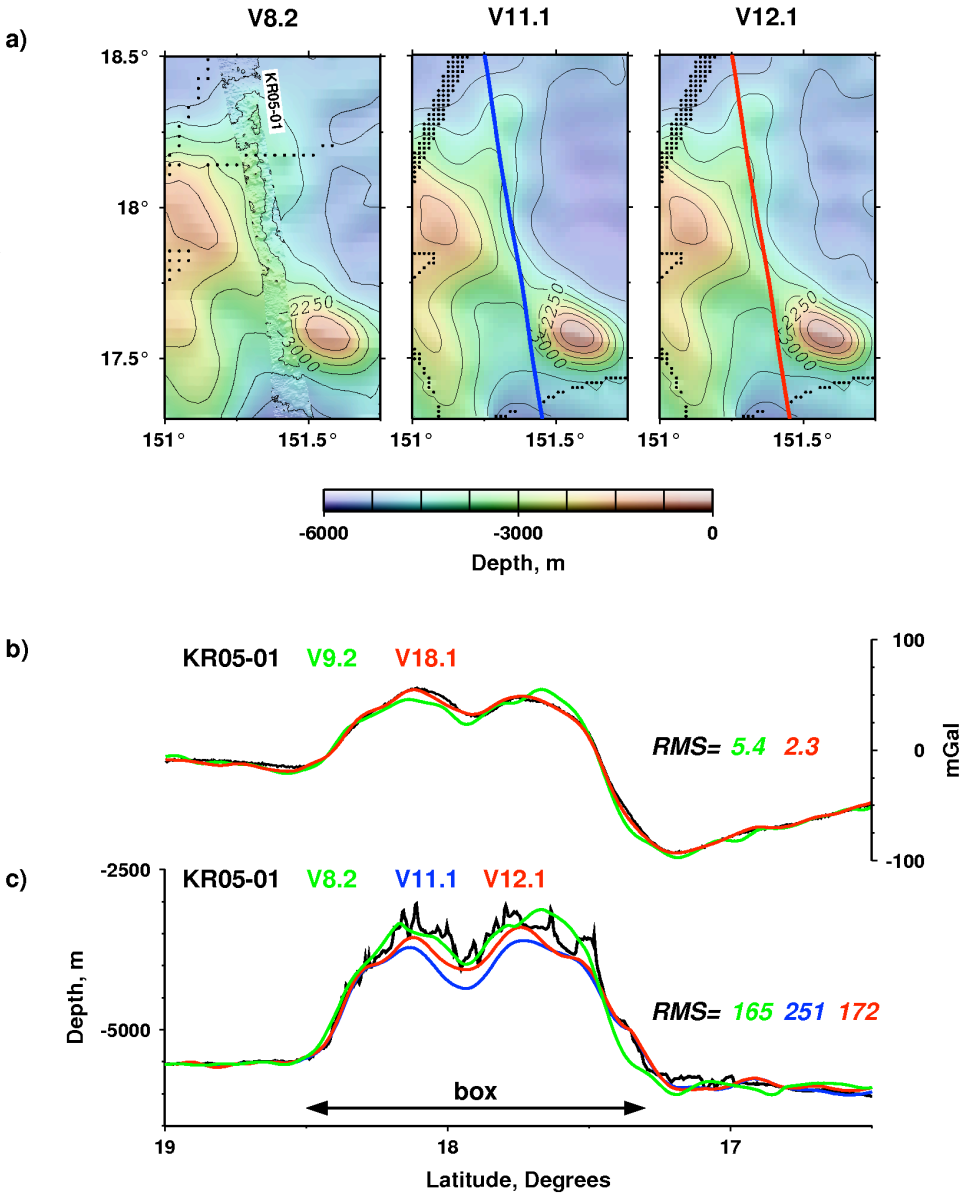

Fig. 9 **a** Selected bathymetry model versions over rough seafloor. KR05-01 multibeam data are plotted on version 8.2; contours show more detail over higher resolution multibeam; model depths match soundings well. Gravity (**b**) and bathymetry (**c**) profiles plotted along KR05-01 center-beam track. Satellite gravity version 18.1 and bathymetry version 8.2 have lowest RMS (defined in Fig. 6 caption) values. Non-linear prediction algorithm used in version 8.2 captures seamount

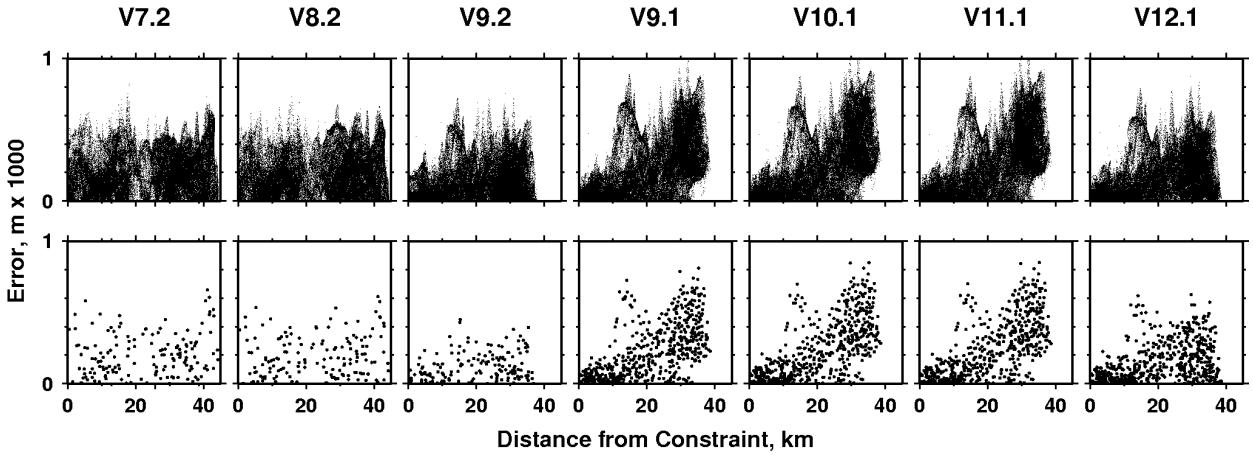

Fig. 10 Errors same as defined in Fig. 7, but for KR05-01 (located in Fig. 9a) in the rough seafloor area (bathymetry models in Fig. 8a). Errors are largest in versions 9.1, 10.1, and 11.1. A bad ship track along ~18.25°N in versions 7.2 and 8.2 (see Fig. 8a) contributes to errors (track edited out in subsequent versions). Scaling correction in version 12.1 reduces amplitude of errors

Regional long-wavelength errors

In the Pacific Ocean north of the Hawaiian Ridge, there are large areas devoid of sounding constraints that enabled us to discover regional-scale errors that had been building up in successive bathymetry models. In Fig. 11a, we plot the differences in depth between version 11.1, and the companion version of 11.1 that we computed withholding JAMSTEC multibeam data. We see there are long-wavelength depth differences that extend even through constraints that are common to both solutions, which is not an expected result. This indicates that version 11.1 without JAMSTEC data contains long-wavelength errors in depth that become evident when compared to the better-constrained version 11.1 that incorporated the JAMSTEC data. The implication is, however, that wherever there are large voids in ship constraints, there may be regional-scale depth errors.

We determined that these long-wavelength errors are the result of basing a bathymetry model version on the previous one, in other words, using low-pass filtered depths from the previous version, instead of recomputing a new regional depth field each time. This can contribute to the amplification of errors seen in successive bathymetry versions 9 through 11 (see Figs. 7 and 10) also.

To demonstrate that this is the cause of the regional errors, we compare version 12.1 that has the gravity-to-topography scaling factor correction discussed earlier and is initiated from S2004, to the companion version 12.1 that had JAMSTEC withheld. In Fig. 11b we see that the long-wavelength depth errors are greatly reduced in version 12.1 and that the differences remain a short distance away from the JAMSTEC swath paths, which is an expected result. The depth differences can be quantified by their standard deviation, σ = 64.1 m for version 11.1, and σ = 43.7 m for version 12.1.

The improvements in version 12.1 are also quantified in Figs. 7 and 10. In these figures, the amplification of errors over successive versions 9 through 11, is not present in 12.1. Instead, version 12.1 has smaller errors over both smooth and rough seafloor.

Concluding Remarks

Overall, the bathymetry models are improving with successive version. Much of this can be attributed to the increasing number of soundings being incorporated into the models and to an improved satellite gravity model. Significantly, we find there is no systematic variation between bathymetry model errors and depth. Our examination of local study areas having large gaps between surveys has revealed problems with the prediction algorithm that are not evident when errors are analyzed on a global scale.

The efforts described in this paper reveal that the newer models (through version 11.1) were in some ways not as good as version 8.2. One problem was traced to the use of the 1-min, as opposed to 2-min, bathymetry grid: the spectral content of the 2-min bathymetry was close to that of the high-cut gravity, so the scaling worked well on a 2-min grid. However a 1-min grid allowed for extra bathymetric variance not captured in the gravity, biasing the scaling of milliGals into meters. This was mitigated in version 12.1 by high-cut filtering the bathymetry before making the correlation and scaling analysis. A second problem was that the long-wavelength trend surface had not

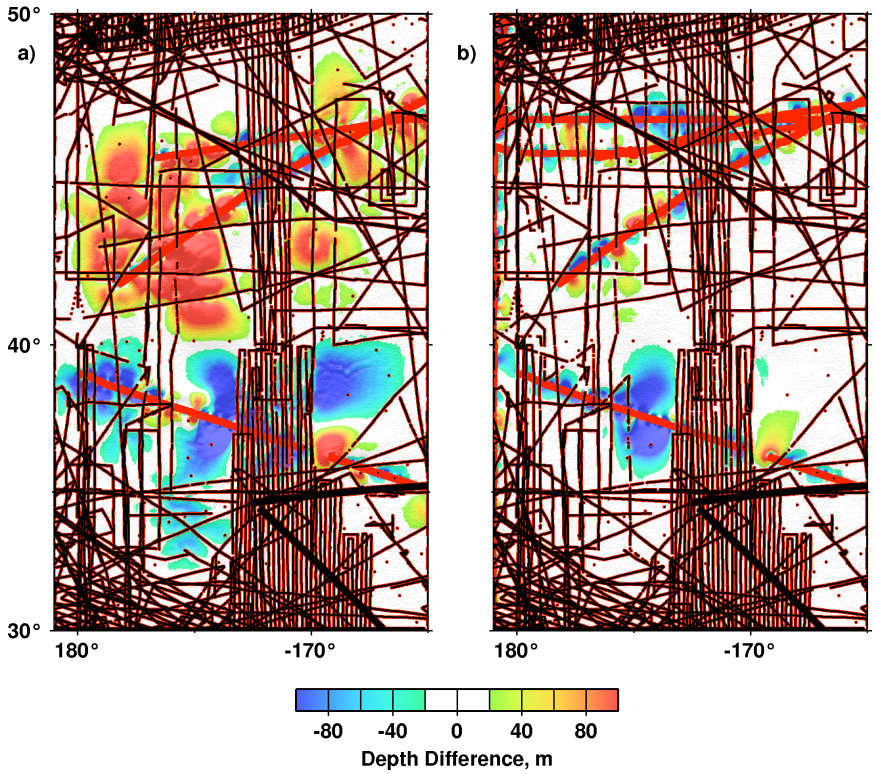

Fig. 11 **a** Depth differences are between version 11.1 with JAMSTEC data (*red dots* are constraints), and version 11.1 with JAMSTEC withheld (*black dots* are constraints). Long-wavelength depth differences can extend even through common constraints. **b** Same as (**a**), except using version 12.1, that has corrected gravity-to-topography scaling and is initiated from S2004. Regional-scale errors have been greatly reduced

been improving as expected, when it was based on a low-pass filter of the previous version. For version 12.1 the long-wavelength surface was based on S2004, which is a blend of GEBCO (British Oceanographic Data Center 2003) in shallow water and polar regions, with version 8.2 in deep water areas equatorward of ±72˚ latitude. Although it seems that the altimetry should be limited by the band-pass filter and so should not alter the long wavelengths, in fact the non-linear approach used in version 8.2, by allowing non-linear growth in the power in the prediction band, allows changes to occur at long wavelengths outside the band. In effect, tall seamounts can change the regional mean depth in version 8.2 differently than they do in the other versions. Version 12.1, by reverting to the long wavelengths of version 8.2, gives a better fit to the new JAMSTEC data.

The current bathymetric model (version 12.1), that has the scaling and long-wavelength problems corrected, can resolve features of the seafloor as small as 18 km across. Yet the spectral analyses of geophysical data measured by ship along a survey in the western Pacific Ocean demonstrates that even shorter wavelengths can be resolved. If the satellite gravity field can be improved, or if a new satellite mission capable of collecting higher-resolution altimetry data were flown, then the resulting bathymetry model could map surprisingly small details of the seafloor- potentially as small as 5 km half-wavelength. Further, future prediction techniques may include the non-linear and threshold-setting algorithm that was used in version 8.2 that apparently produced a superior bathymetric prediction than even more recent versions. When this feature and other improvements are made, future bathymetry model versions will be greatly improved.

Acknowledgements Data and web applications discussed in this paper are available at the following websites: Smith and Sandwell's (1997) altimetric bathymetry grid V12.1 (http://topex.ucsd.edu/WWW_html/mar_topo.html), SRTM30_Plus V6.0 (http://topex.ucsd.edu/WWW_html/srtm30_plus.html), GEBCO_08 bathymetry grid version 20091120, (http://www.gebco.net), Google Earth (http://earth.google.com), and JAMSTEC multibeam data (http://www.godac.jamstec.go.jp/cruisedata/e/). Data used in this study were acquired during the KR05-01 cruise of R/V KAIREI and the MR06-01 cruise of R/V MIRAI, Japan Agency for Marine-Earth Science and Technology. We thank JAMSTEC for making multibeam echo sounder data freely available. The comments of two anonymous reviewers improved this manuscript. The views, opinions, and findings contained in this report are those of the authors and should not be construed as an official National Oceanic and Atmospheric Administration or U.S. Government position, policy, or decision.

This article is available online at:
http://www.springer.com/earth+sciences+and+geography/oceanography/journal/11001

References

Baudry N, Calmant S (1991) 3-D modelling of seamount topography from satellite altimetry. Geophys Res Lett 18:1143-1146. doi:10.1029/91GL01341

Becker JJ, Sandwell DT, Smith WHF, Braud J, Binder B, Depner J, Fabre D, Factor J, Ingalls S, Kim S-H, Ladner R, Marks K, Nelson S, Pharaoh A, Trimmer R, Von Rosenburg J, Wallace G, Weatherall P (2009) Global bathymetry and elevation data at 30 arc seconds resolution: SRTM30_PLUS. Mar Geod 32:355-371. doi:10.1080/01490410903297766

Bendat JS, Piersol AG (1986) Random data: analysis and measurement procedures, 2nd edn. Wiley, New York

British Oceanographic Data Center (2003) Centenary edition of the GEBCO digital atlas [CD-ROM]. Published on behalf of the Intergovernmental Oceanographic Commission and the International Hydrographic Organization, Liverpool

Calmant S (1994) Seamount topography by least-squares inversion of altimetric geoid heights and shipborne profiles of bathymetry and/or gravity. Geophys J Int 119:428-452. doi:10.1111/j.1365-246X.1994.tb00133.x

Goff JA, Smith WHF (2003) A correspondence of altimetric gravity texture to abyssal hill morphology along the flanks of the Southeast Indian ridge. Geophys Res Lett 30:24 doi:10.1029/2003GL018913.

Goff JA, Smith WHF, Marks KM (2004) The contributions of abyssal hill morphology and noise to altimetry gravity fabric. Oceanography 17:24-37

Jakobsson M, Macnab R, Mayer L, Anderson R, Edwards M, Hatzky J, Schenke H-W, Johnson P (2008) An improved bathymetric portrayal of the Arctic Ocean: implications for ocean modeling and geological, geophysical and oceanographic analysis. Geophys Res Lett 35:L07602. doi:10.1029/2008GL033520

Jung W-Y, Vogt PR (1992) Predicting bathymetry from Geosat-ERM and shipborne profiles in the South Atlantic Ocean, Tectonophysics 210:235-253. doi:10.1016/0040-1951(92)90324-Y

Marks KM, Smith WHF (2006) An evaluation of publicly available global bathymetry grids. Mar Geophys Res 27:19-34. doi:10.1007/s11001-005-2095-4

Marks KM, Smith WHF (2007) Some remarks on resolving seamounts in satellite gravity. Geophys Res Lett 34:L03307, doi:10.1029/2006GL028857

Marks KM, Smith WHF (2009) An uncertainty model for deep ocean single beam and multibeam echo sounder data. Mar Geophys Res 29:239-250. doi:10.1007/s11001-008-9060-y

Oldenburg DW (1974) The inversion and interpretation of gravity anomalies. Geophysics 39:526-536, doi:10.1190/11440444

Parker RL (1973) The rapid calculation of potential anomalies. Geophys J R Astron Soc 31:447-455. doi:10.1111/j.1365-246X.1973.tb06513.x

Ramillien G, Cazenave A (1997) Global bathymetry derived from altimeter data of the ERS-1 Geodetic Mission. J Geodyn 23:129-149. doi:10.1016/S0264-3707(96)00026-9

Sandwell DT, Smith WHF (1997) Marine gravity anomaly from Geosat and ERS 1 satellite altimetry. J Geophys Res 102:10039-10054. doi:10.1029/96JB03223

Sandwell DT, Smith WHF (2005) Retracking ERS-1 altimeter waveforms for optimal gravity field recovery. Geophys J Int 163:79-89. doi:10.1111/j.1365-246X.2005.02724.x

Sandwell DT, Smith WHF (2009) Global marine gravity from retracked Geosat and ERS-1 altimetry: ridge segmentation versus spreading rate, J Geophys Res 114:B01411. doi:10.1029/2008JB006008

Sichoix L, Bonneville A (1996) Prediction of bathymetry in French Polynesia constrained by shipboard data. Geophys Res Lett 23:2469-2472. doi:10.1029/96GL02122

Smith WHF (1993) On the accuracy of digital bathymetric data. J Gephys Res 98(B6):9591-9603. doi:10.1029/93JB00716

Smith WHF, Sandwell DT (1994) Bathymetric prediction from dense satellite altimetry and sparse shipboard bathymetry. J Geophys Res 99(B11):21803-21824. doi:10.1029/94JB00988

Smith WHF, Sandwell DT (1997), Global sea floor topography from satellite altimetry and ship depth soundings. Science 277:1956-1962. doi:10.1126/science.277.5334.1956

Wessel P, Smith WHF (1998) New, improved version of Generic Mapping Tools released. EOS Trans AGU 79:579. doi:10.1029/98EO00426

Wessel P, Watts A (1988) On the accuracy of gravity measurements. J Geophys Res 93(B1):393-413. doi:10.1029/JB093iB01p00393